Conference Paper, Published Version

Kuhnle, Roger; Jia, Yafei; Alonso, Carlos

3-Diemnsional Measured and Sumulated Flow of Scour Near Spur Dikes

3-Dimensional Measured and Simulated Flow for Scour Near Spur Dikes

Roger Kuhnle[1], Yafei Jia[2], and Carlos Alonso[3]

ABSTRACT

To improve understanding of the flow and scour processes associated with spur dikes more fully, 3-dimensional flow velocities were measured using an acoustic Doppler velocimeter at a closely spaced grid over a fixed flat bed with a submerged spur dike. Some 2592 three-dimensional velocities around a trapezoidal shaped submerged spur dike were measured. General velocity distribution and detailed near field flow structures were revealed by the measurement. Some important differences between the flow fields measured in this study and those measured for non-submerged vertical obstructions were observed in this study. Numerical simulation was performed using the free surface turbulent flow model, CCHE3D. The numerical simulation of the flow showed very good agreement between the computation results and the measurements. The numerical simulation results indicate the CCHE3D model can be used to predict near-field flows around hydraulic structures.

Keywords: *submerged spur dike, 3-dimensional flow, velocity measurements, 3-dimensional modeling, free surface flow, hydraulic structure*

INTRODUCTION

A spur dike may be defined as a structure extending outward from the bank of a stream for the purpose of deflecting the current away from the bank to protect it from erosion. Where the bank material is erodible, streams and rivers often erode the banks and move laterally, resulting in land loss, channel change, excessive sediment yield and degradation of the water quality. The use of a series of spur dikes is one of the most effective means of stabilizing or realigning channel banks. For economic reasons, spur dikes are often constructed of riprap and are commonly designed to be submerged during high flows. The pools formed from the local scour associated with spur dikes have been used successfully to enhance aquatic habitat in unstable streams (Shields et al., 1995). Despite the widespread use of spur dikes, many aspects of their design are based on prior experience and are only applicable to streams of a similar nature (e. g. Copeland, 1983). An improved understanding of the complicated 3-D flow in the vicinity of spur dikes and its interaction with the entrainment and transport of sediment is needed.

[1] Research Hydraulic Engineer, National Sedimentation Laboratory, USDA, Agricultural Research Service, P. O. Box 1157, Oxford, Mississippi 38655, USA. Email: rkuhnle@ars.usda.gov.
[2] Research Associate Professor, National Center for Computational Hydroscience and Engineering, The University of Mississippi 38677, USA. Email: jia@ncche.olemiss.edu.
[3]Research Leader, Channel and Watershed Processes Research Unit, National Sedimentation Laboratory, USDA, Agricultural Research Service, P. O. Box 1157, Oxford, Mississippi 38655, USA. Email: calonso@ars.usda.gov.

There have been few previous studies of the flow in the vicinity of spur dikes. Rajaratnam and Nwachukwu (1983) studied the flow in a laboratory flume near groin-like structures represented by an aluminum plate which projected above the water surface. A pitot-static tube was used to measure the flow in regions of undisturbed flow and a three-tube yaw probe was used in regions of skewed flow. They found that the bed shear stresses at the upstream corner of the plate were up to five times the bed shear stresses in the approach flow section. The initiation of local scour is associated with the increase in shear stress caused by the accelerating flow around the obstruction. For cylindrical bridge piers, scour has been observed to be dominated by a strong downflow on the upstream side of the pier and a horseshoe vortex which surrounds the upstream and lateral sides of the pier (e.g. Mellville and Raudkivi, 1977; Graf and Yulistiyanto, 1998; Istiyato and Graf, 2001). For bridge abutments, which are in many ways similar to spur dikes, flow features resembling those observed around one-half of a cylindrical bridge pier have been measured, including the primary vortex (essentially one half of the horse-shoe vortex), which forms around the structure and contributes to the development of scour (Kwan and Melville, 1994). These investigators have determined that the flow structures around a model wingwall abutment are dominated by the large primary vortex and an associated downflow.

Detailed velocity measurements around a submerged spur dike with a trapezoidal shape are rare. Flow around this structure would be expected to vary from that of flat plates and abutments due to the over-topping flow and 3-dimensional shape of the structure. The over-topping flow and trapezoidal shape would be expected to affect the characteristics of the primary vortex and make the recirculation zone behind the spur dike more three-dimensional. Because the flow is the key to understanding the performance of a submerged spur dike, the velocity field around the spur dike was measured in a laboratory flume at the National Sedimentation Laboratory. This data set of 2592 point measurements was compared to flow simulations calculated using the 3-dimensional numerical flow model (CCHE3D) developed at the National Center for Computational Hydroscience and Engineering, University of Mississippi.

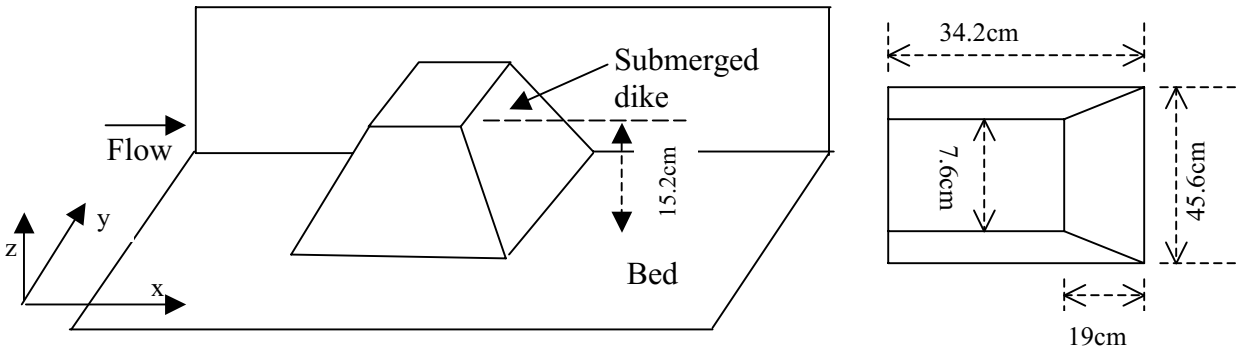

Fig. 1. Sketch of the model spur dike (not to scale) used in the experiments.

PHYSICAL MODEL AND VELOCITY DATA

All of the flow measurements were collected in a recirculating flume with a test channel 30 m long, 1.2 m wide, and 0.6 m deep located at the National Sedimentation Laboratory. Flow rate in the flume was measured using a pressure transducer connected to a Venturi meter in the return

Table 1. Flow condition of the flume experiments.

Exp. Run	Flow rate (m^3/s)	Flow depth (m)	Mean Flow velocity (m/s)	Froude Number
Flat fixed bed	0.129	0.3048	0.347	0.201

pipe. Flow depth was controlled by the amount of water in the flume and measured by taking the difference in elevation between 12-m long bed and water surface transects in the approach flow section. The bed of the approach flow section was covered with sediment (D_{50} = 0.8 mm, $[D_{84}/D_{16}]^{1/2}$ =1.35). The bed sediment was immobilized with a thin layer of cement from 21.9 m downstream of the channel inlet to the tail box to prevent the bed from changing. The zero location of the *x* (streamwise) coordinate was located 22.6 m downstream of the channel inlet and the center of the spur dike model was located 1.19 m downstream from the zero coordinate. The spur dike model (Fig. 1) was located on the left wall of the channel facing downstream. Flow conditions were very similar to those used in one experiment from Kuhnle, et al. (1999) and are summarized in Table 1. The ratio of the flow shear stress to the critical shear stress of the bed material sediment obtained from the Shields (1936) curve was 0.7 in the approach flow section.

The velocity data was collected using a commercially available Acoustic Doppler Velocimeter (ADV). The measurement head of the ADV is mounted on a stainless steel mast 60 cm long and 1 cm in diameter. The measurement head has three sensors mounted at a spacing of 120° around a circle approximately 7 cm in diameter. The sampling volume of the ADV is a cylinder 6 mm in height and 6 mm in diameter (170 mm^3) located 5 cm away from the head of the ADV. Flow velocity data at each point was collected at 50 Hz for 5 minutes. The 5 minute sample duration was determined empirically as the optimum length of time to capture the mean velocity at the sampling location within a reasonable time frame. The relatively large measurement volume and low rate of data acquisition of ADVs when compared to laser Doppler anemometers, indicate that the higher frequency and smaller scales of flow turbulence cannot be adequately measured using an ADV.

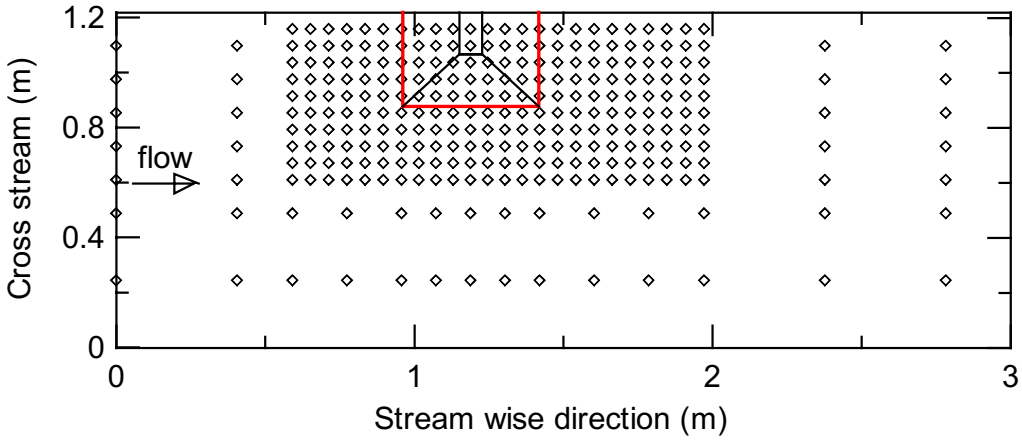

Fig. 2. Plan view of experimental flume with measurement locations indicated by diamond symbols. Outline of base of spur dike shown in red.

Flow velocities were measured at 288 locations as shown in Figure 2. At each location the flow was measured at 9 vertical positions: 0.0100, 0.0225, 0.0350, 0.0475, 0.0600, 0.1000, 0.1400,

0.1800, and 0.2200 m from the bed. The vertical measurement positions were adjusted accordingly at the locations above the spur dike to arrive at nine measurement positions. A total of 2592 velocity vectors were measured. All velocity records were processed using the public domain program, WinADV. Measurements were filtered using WinADV to reject points with a correlation coefficient less than 0.7. In most files 90% or more of the data was above 0.7.

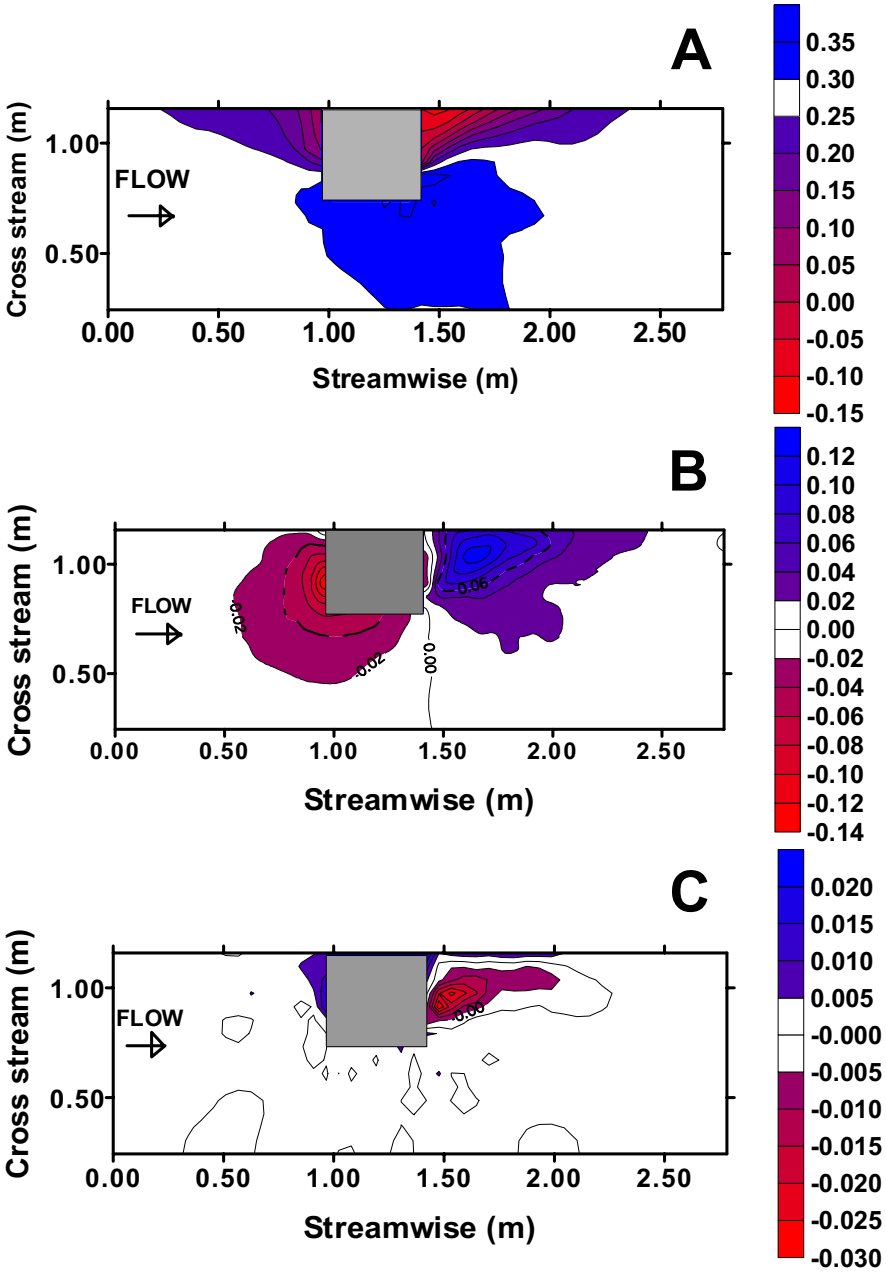

Fig. 3. Contours of flow velocity (m/s) for the plane 0.01 m above the bed, (A) u - streamwise velocity, (B) v - cross-stream velocity, and (C) w - vertical velocity. Gray area represents the outline of the model spur dike at the bed.

GENERALIZED VELOCITY DATA

The general trends of flow velocities in the plane 0.01 m from the bed are shown in Figure 3. Streamwise velocity is shown to increase in magnitude on the right side of the spur dike while decreasing and becoming negative upstream of and in the lee of the structure. Cross-stream velocity is directed around and over the structure (Fig. 3B), and vertical velocity (Fig. 3C) is affected upstream and downstream of the structure as the flow converges and diverges over the top of the structure. In Figure 4 the root mean square of the deviations in *u* are shown to decrease as the flow accelerates around the structure, and to be the greatest in the region downstream of the structure where the flow separates from the boundary. Contour plots for *v*- and *w*-fluctuations were similar to Figure 4. A salient aspect of these results stems from the fact that the structure being trapezoidal in shape and submerged generates a flow pattern that does not "pile up" on the upstream edge of the structure, and the separation zone is more complicated because flow is converging from more than one direction as compared with other studies (Rajaratnam and Nwachukwu, 1983; Kwan and Melville, 1994).

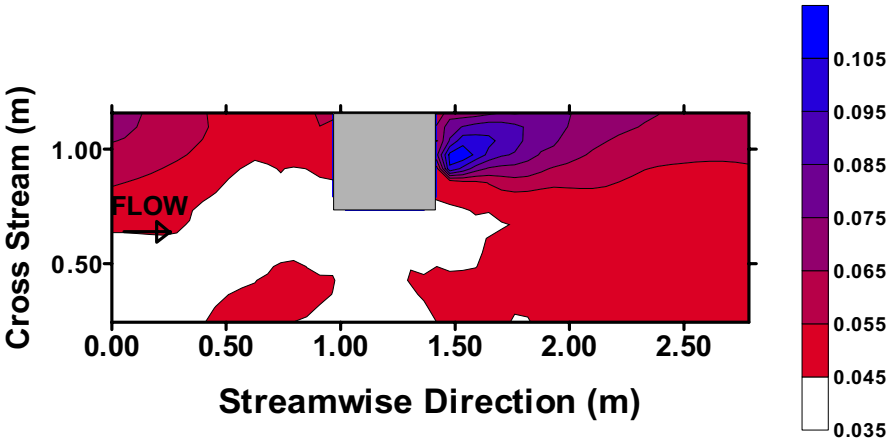

Fig. 4. Contours of root mean square of deviations in u, at plane 0.01 m above the bed.

NUMERICAL SIMULATION MODEL

Numerical simulations of three-dimensional free surface flow around hydraulic structures have been attempted with reasonable success (Jia and Wang 1996, 1999, Richardson, and Punchang, 1998). The three-dimensional, unsteady, turbulent free surface flow model, CCHE3D, has been applied to simulate the flow around submerged spur dikes in this study. This model has been applied (Jia and Wang, 2000) to simulate a similar experimental case conducted by Kuhnle et al. (1997), to study flow field and local scouring without measured velocity data. This model uses the finite element method to solve the following governing equations.

The Reynolds stress equations:

$$u_{i,t} + u_j u_{i,j} - (-\overline{u_i u_j})_{,j} + \frac{p_i}{\rho} + f_i = 0 \tag{1}$$

$$u_{j,j} = 0 \tag{2}$$

where u represents the mean velocity, u' represents the turbulent velocity fluctuation, p is the mean pressure, ρ is the density of the water, and f is the gravitational force.

The free surface kinematic equation:

$$\frac{\partial \eta}{\partial t} + u_\eta \frac{\partial \eta}{\partial x} + v_\eta \frac{\partial \eta}{\partial y} + w_\eta = 0 \tag{3}$$

where η denotes the free surface elevation.

The k-ε turbulence closure scheme:

$$k_{,t} + u_j k_{,j} - (\frac{\nu_k}{\sigma_k} k_{,j})_{,j} = P - \varepsilon \tag{4}$$

$$\varepsilon_{,t} + u_j \varepsilon_{,j} - (\frac{\nu_k}{\sigma_\varepsilon} \varepsilon_{,j})_{,j} = c_{\varepsilon 1} P \frac{\varepsilon}{k} - c_{\varepsilon 2} \frac{\varepsilon}{k^2} \tag{5}$$

where k represents the turbulent kinetic energy $u_i' u_i'/2$, ε represents the rate of dissipation of turbulent kinetic energy, ν_t denotes the turbulent viscosity given by:

$$\nu_t = c_\mu \frac{k^2}{\varepsilon} \tag{6}$$

and P is the production of turbulent kinetic energy computed from:

$$P = \nu_t (u_{,j} + u_{,i}) u_{,i} \tag{7}$$

The values of empirical coefficients appearing in the preceding equations were assigned c_μ=0.09, σ_k=1.0, σ_ε=1.3, $c_{\varepsilon 1}$=1.44, $c_{\varepsilon 2}$=1.92.

The velocity correction method was used to solve the momentum equations (Jia et al, 2001). A Poisson's equation formulated with the velocity correction terms and the continuity equation was solved on a staggered grid to obtain the dynamic pressure and force the flow to satisfy the divergence free condition. Wall boundary conditions were used for the momentum equations and the k-ε closure model. The shape of the spur dike is trapezoidal in cross-sectional and longitudinal directions with very steep slopes, a body fitted 3D grid was generated over the dike. The system of equations was solved implicitly by using the SIP method with the first order Euler's scheme.

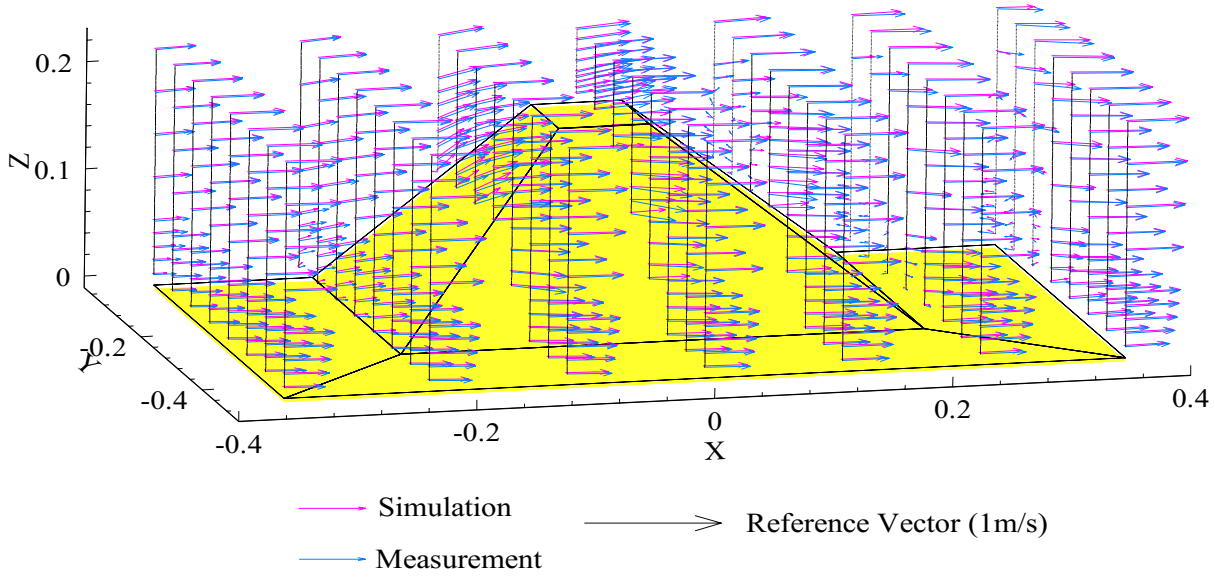

Fig. 5. A perspective view of simulated and measured flow field around the submerged spur dike.

SIMULATION RESULTS

Figure 5 shows a perspective view of the trapezoidal-shaped spur dike and the simulated and measured velocities in this study. The far side (Y=0) is where the vertical wall of the flume is, and the horizontal plane is the channel bed. To focus attention and make the comparison clear, the area shown in the figure is only the close vicinity of the spur dike, and all other measured locations are ignored. The spur dike (Fig. 5) is surrounded by a field of measured and computed velocity vectors, with all the data in the seven cross sections displayed. Two velocity vectors are drawn at each point along a vertical line. The vectors in blue represent measured velocities and those in red represent the simulated velocities at the same location. Because the spatial locations of measuring points differ from mesh points of the computation, linear interpolation was applied to estimate the simulated velocity at the measuring locations. Generally, the flow field of the physical model is well reproduced by the numerical simulation. The velocity magnitude and direction of most simulated vectors agree with those measured. It is noted though, larger differences appear at several places: the corner near the wall and bed in the upstream side; in the recirculation zone downstream of the spur dike, and on the upper part of the spur dike slopes. For vectors of smaller magnitude, the relative differences appear larger.

Figure 6 shows the comparison of the computed and measured total velocity magnitude. The diagonal line represents the perfect agreement. It can be seen that the numerical prediction reproduced the physical model data with very little systematic error (r^2=0.97). The error norm for the total velocity

$$\sigma = \frac{1}{N}\sum\sqrt{\left|U_s^2 - U_m^2\right|} \approx 0.0825 \tag{8}$$

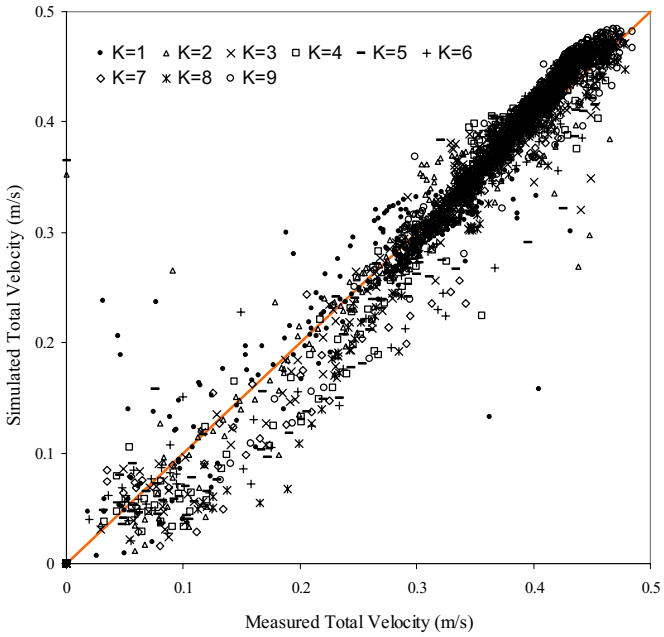

Fig. 6. Comparison of the simulated and measured total velocity magnitude. K=1, K=2, … K=9 indicate the vertical level of measurement with K=1 represents the level near the bed and K=9 represents the level near the surface.

is reasonably small with U_s and U_m representing simulated and measured total velocity and N=2592. The point scattering is slightly higher for smaller velocities (<0.3m/s). Most of the points which scatter farther away from the diagonal line are those close to the bed or spur dike surface. This scattering reflects the difficulty of measuring acoustic data close to a solid surface.

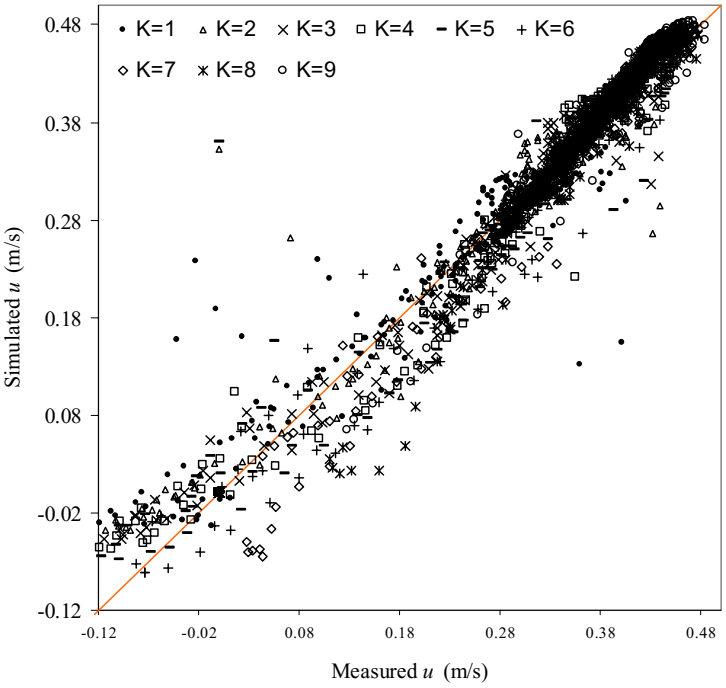

Fig. 7. Comparison of simulated and measured *u* velocity component (R^2=0.970). K=1, K=2, … K=9 indicate the vertical level of measurement with K=1 represents the level near the bed and K=9 represents the level near the surface.

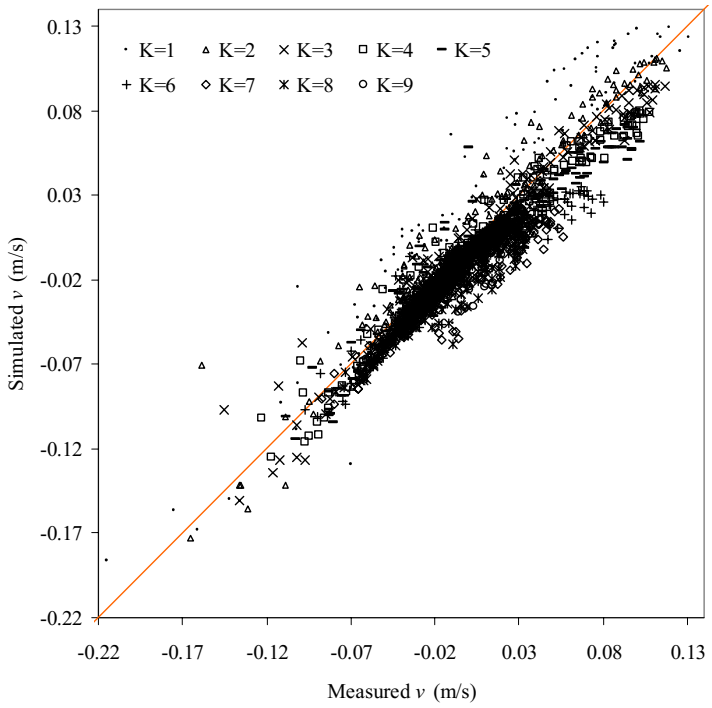

Fig. 8. Comparison of simulated and measured *v* velocity component (R^2=0.886). K=1, K=2, … K=9 indicate the vertical level of measurement with K=1 represents the level near the bed and K=9 represents the level near the surface.

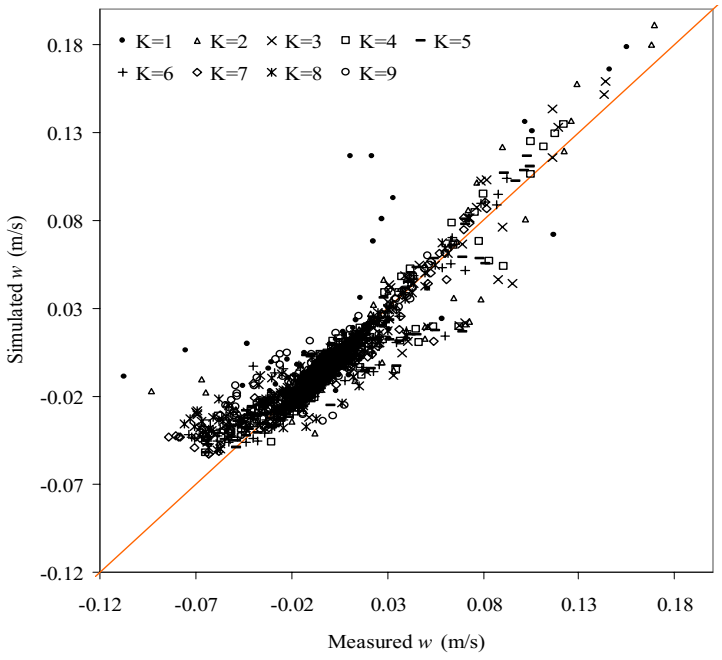

Fig. 9. Comparison of simulated and measured *w* velocity component (R^2=0.834). K=1, K=2, … K=9 indicate the vertical level of measurement with K=1 represents the level near the bed and K=9 represents the level near the surface.

Figures 7, 8, and 9 show comparisons of simulated velocity components *u, v*, and *w* individually. As shown in Figure 1, *u, v* and *w* are the longitudinal, transverse and vertical components, respectively. The *v* component is seen to be distributed along the diagonal without skew but scattering is wider for the range $v>0$ (Fig. 8). *u* and *w* components are a little under predicted when they have negative values (Fig. 7 and 9).

Since the *u* component is negative, *v* component is positive only in the recirculation zone, and the negative *w* component values distribute mainly behind the spur dike, these differences therefore are mainly in the recirculation zone. At other locations the prediction and the measurement are consistent without obvious systematic errors.

The comparisons of simulated and measured transverse velocity (secondary currents) in cross-sections around the spur dike are shown in Figure 10. To facilitate the visual comparisons, alternate sections are plotted separately in two plots. Although differences between the simulations and measurements can be observed, the general patterns of secondary flows agree very well. The agreement in the front and middle sections is better than behind the spur dike. In the recirculation zone, the general directions and magnitude of the secondary flow vectors are simulated quite well, however, the magnitude of vertical velocity components away from the bed are under-estimated, and, thus the angles between the simulation and measured vectors are relatively large.

Velocities projected on longitudinal sections (*u*-*w*) are plotted in Figure 11. To enhance clarity, alternate sections are drawn in separate plots (a) and (b). The perspective view is from outside the wall attaching the spur dike and from downstream to upstream. The comparisons in the figure indicate that the re-circulation downstream of the spur dike, driven by the overtop shear flow, is simulated very well, although reverse flow velocities are weaker than those measured. The simulated velocity vectors in these sections in general exhibit little differences from the measured ones. In the front corner near the wall and bed, the predicted velocity is smaller than the measured, and the primary vortex that has been observed in spur dikes with vertical front wall and abutment models is not observed in this case. This is why the skews appear at the lower end of Figures 7 and 9.

The flow direction and general pattern are illustrated by velocity vectors and particle path lines in Figure 12. The secondary flows around the spur dike include a small vortex in the front corner and a larger recirculation cell behind the spur dike. The high shear stress zone on the channel bed indicates the potential location of the scour hole. Unlike the flow around obstructions with vertical walls, the flow around the submerged trapezoidal spur dike has a fully three-dimensional recirculation cell. For structures with a vertical front, the blockage to the oncoming flow usually creates a strong down-flow and primary or horseshoe vortex. This has been observed in studies of cylindrical piers and bridge abutments (Melville and Raudkivi, 1977; Kwan and Melville, 1994; Graf and Yulistiyanto, 1998). The down-flow in front of this trapezoidal shaped submerged spur dike, however, is almost not present as the flow instead moves upwards along the surface of the spur dike, except close to the bed and near the corner of the wall where a small vortex is generated. The primary vortex measured and recognized by Kwan and Melville (1994) was not observed in this study.

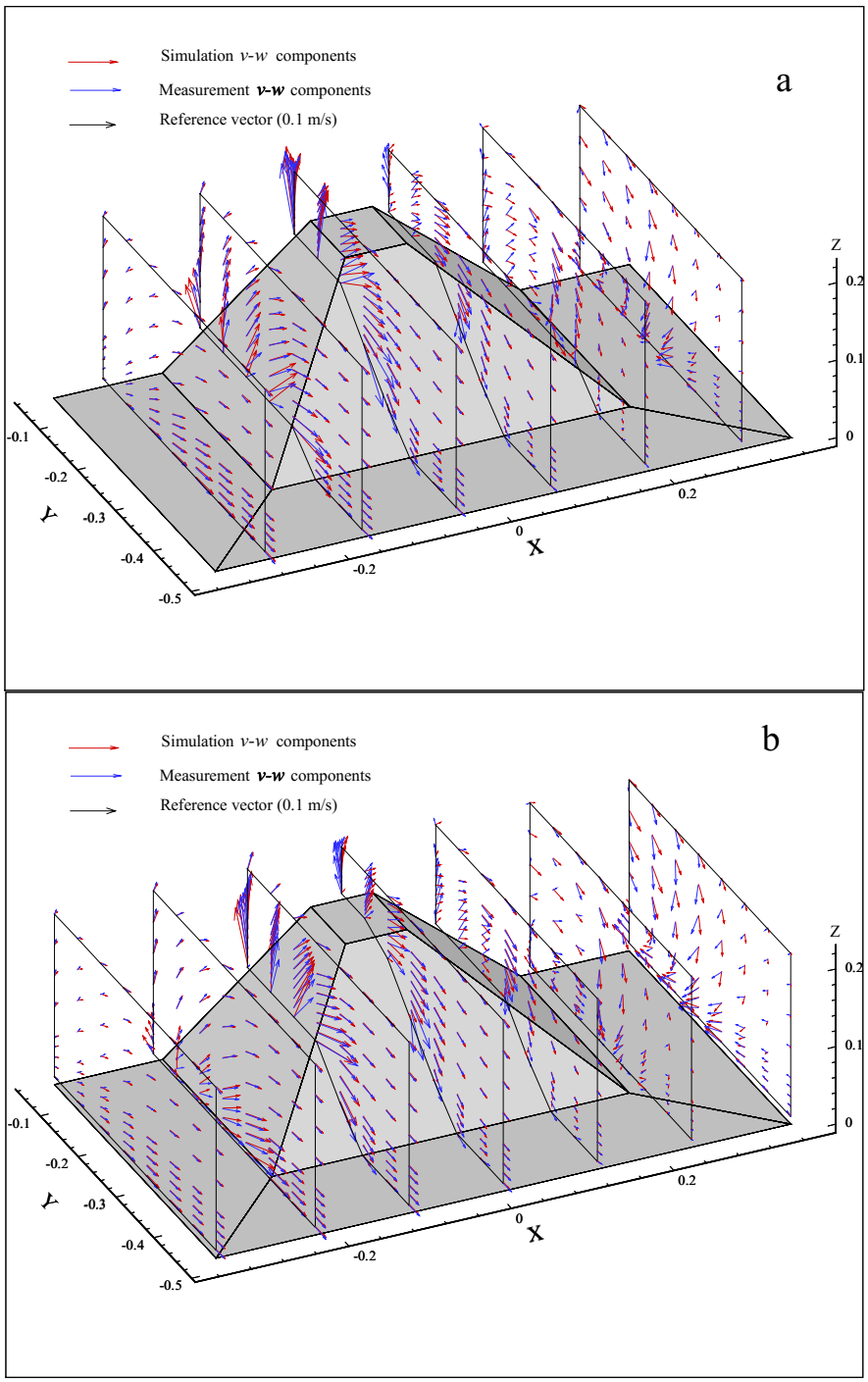

Fig. 10. Comparison of simulated and measured transverse velocity (*v*-*w*) components in cross-sections around the spur dike at the locations (a) x = 0.8961, 1.0150, 1.1308, 1.2466, 1.3625, 1.4813 m; (b) x = 0.8352, 0.9571, 1.0729, 1.1887, 1.3045, 1.4204, 1.5423 m, shown in Fig. 2.

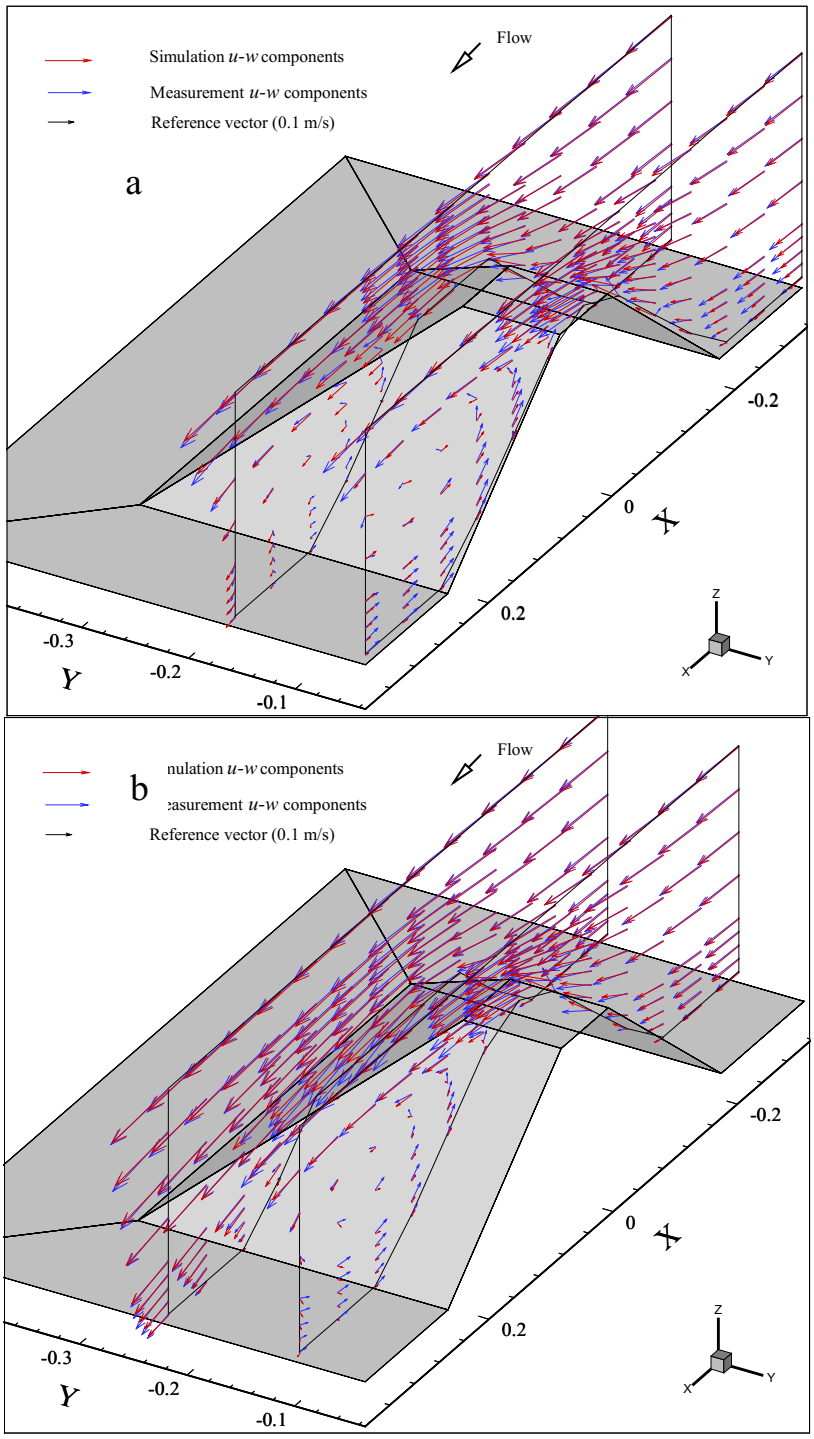

Fig. 11. Comparisons of simulated and measured flow pattern (*u-w*) in longitudinal sections: (a) y = 1.1582, 1.0363 m; (b) y = 1.0973, 0.9754 m, shown in Figure 2.

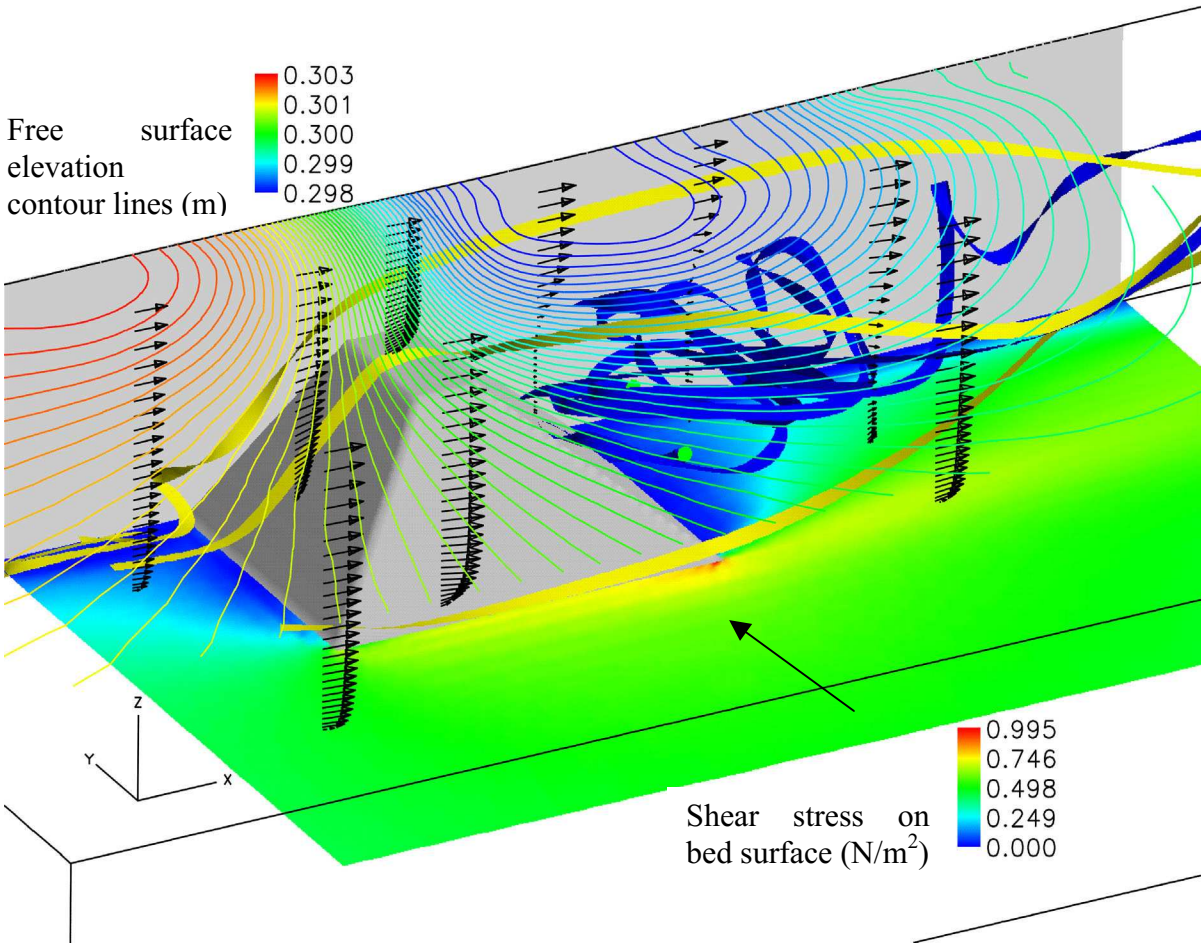

Fig. 12. Simulated near field flow pattern around the submerged spur dike. Yellow ribbons are released in front of the spur dike, blue ones are released from behind. The shear stress distribution on the bed is shown by color shading (red – high; yellow – low).

CONCLUSIONS

Three dimensional flow measurements around a model spur dike with a stationary bed showed little or no evidence for a strong downflow on the upstream side or a primary vortex. These features have been described in other studies of piers, dikes and abutments. The differences in flow features observed is believed to be the result of the 3-dimensional shape of the model spur dike and the over-topping flow used in this study.

The three-dimensional finite element model for free-surface and turbulent flow (CCHE3D) was used to simulate the flow around the submerged spur dike. The agreement between the simulation results and the observations is very good, although some discrepancy is noted downstream of the spur dike in the recirculation zone. The error norm of the comparison for the whole data set is 8.25%. These results indicate that the CCHE3D model can yield robust simulations of velocity flow patterns around hydraulic structures of complex shape such as the

trapezoidal submerged spur dike used in this study. Use of computational models, such as CCHE3D, have the potential to improve the design of spur dikes for erosion control projects.

ACKNOWLEDGMENTS

This work is a result of research supported in part by the USDA Agriculture Research Service under Specific Research Agreement No. 58-6408-7-035 (monitored by the USDA-ARS National Sedimentation Laboratory) and The University of Mississippi. Research Assistant, T.T. Zhu, helped to produce many of the figures. John Cox and Emery Sayre collected the flow data that was used in this paper. John Cox carried out the initial processing of the flow data.

REFERENCES

Copeland, R. R., 1983, "Bank protection techniques using spur dikes." Miscellaneous Paper HL-83-1, U. S. Army Waterways Experiment Station, Vicksburg, Mississippi, 32 pp.

Graf, W.H., and Yulistiyanto, B., 1998, "Experiments on flow around a cylinder; the velocity and vorticity fields", Journal of Hydraulic Research, IAHR, 36(4), 637-653.

Istiyato, I., Graf, W.H., 2001, "Experiments on flow around a cylinder in a scoured channel bed", International Journal of Sediment Research, Vol. 16, No. 4, pp431-444.

Jia, Y., and Wang, S.S.Y., 1996, "A modeling approach to predict local scour around spur dike-like structures", Proceedings of the Sixth Federal Interagency Sedimentation Conference, p. II-90-97.

Jia, Y., and Wang, S.S.Y., 1999, "Simulation of horse-shoe vortex around a bridge pier", Proceedings of the International Water Resources Engineering Conference". CD-ROM, 10 pp.

Jia, Y., and Wang, S.S.Y., 2000, **"**Numerical Study of Turbulent Flow around Submerged Spur Dikes", 4th International Conference for Hydroscience and Engineering, 2000, Seoul, Korea.

Jia, Y., Kitamura, T., and Wang, S.S.Y., 2001, "Simulation scour process in a plunge pool with loose material", ASCE, *Journal of Hydraulic Engineering*, Vol. 127, No. 3, pp219-229.

Kuhnle, R., Alonso, C.V., and Shields, F.D., 1997, "Geometry of scour holes around spur dikes, and experimental study", Wang, S.S.Y., Langendoen, E.J., and Shields, F.D., (ed.) Proceedings of the Conference on Management of Landscapes Disturbed by Channel Incision, Center for Computational Hydroscience and Engineering, School of Engineering, The University of Mississippi, p. 283-287.

Kuhnle, R., Alonso, C.V., and Shields, F.D., 1999,"Geometry of scour holes associated with 90^{o} spur dikes", Journal of Hydraulic Engineering, ASCE, 125(9), 972-978.

Kwan, T.F., and Melville, B.W., 1994, "Local scour and flow measurements at bridge abutments", Journal of Hydraulic Research, IAHR, 32(5), 661-673.

Melville, B.M., and Raudkivi, A., 1977, “Flow characteristics in local scour at bridge piers”, Journal of Hydraulic Research, IAHR, 15(4), 373-380.

Rajaratnam, N., and Nwachukwu, B. A. 1983. “Flow near groin-like structures.” Journal of Hydraulic Engineering, ASCE, 109(3), 463-480.

Richardson, J.E., and Punchang, V.G., 1998, “Three dimensional simulation of scour-induced flow at bridge piers”, Journal of Hydraulic Engineering, ASCE, 124(5), 530-540.

Shields, A., 1936, Anwendung der Aenlichkeitsmechanik und der Turbulenzforschung auf die Geschiebebewegung, Mitteilungen der Preussischen Versuchsanstalt fur Wasserbau und Schiffbau, Berlin, Germany, translated to English for W.P. Ott and J.C. van Uchelen, California Institute of Technology, Pasadena, CA.

Shields, F. D., Jr., Cooper, C. M., Knight, S. S., 1995, “Experiment in stream restoration.” Journal of Hydraulic Engineering, ASCE, 121(6), 494-502.